








## Article

# Study on Relationship of Land Cover Changes and Ecohydrological Processes of the Tuul River Basin

Batsuren Dorjsuren <sup>1</sup>, Nyamdavaa Batsaikhan <sup>2,\*</sup>, Denghua Yan <sup>3,\*</sup>, Otgonbayar Yadambjav <sup>4</sup>, Sonomdagva Chonokhuu <sup>1</sup>, Altanbold Enkhbold <sup>2</sup>, Tianlin Qin <sup>3</sup>, Baisha Weng <sup>3</sup>, Wuxia Bi <sup>3</sup>, Otgonbayar Demberel <sup>5</sup>, Tsasanchimeg Boldsaikhan <sup>6</sup>, Oyunkhuu Gombo <sup>7</sup>, Mohammed Gedefaw <sup>8</sup>, Abel Girma <sup>8</sup> and Asaminew Abiyu <sup>8</sup>

- <sup>1</sup> Laboratory of Air and Environmental Monitoring, Department of Environment and Forest Engineering, School of Engineering and Applied Sciences, National University of Mongolia, Ulaanbaatar 210646, Mongolia; batsuren@seas.num.edu.mn (B.D.); ch\_sonomdagva@num.edu.mn (S.C.)
- <sup>2</sup> Department of Geography, School of Art & Sciences, National University of Mongolia, Ulaanbaatar 210646, Mongolia; altanbold@num.edu.mn
- <sup>3</sup> State Key Laboratory of Simulation and Regulation of Water Cycle in River Basin, China Institute of Water Resources and Hydropower Research (IWHR), Beijing 100038, China; qintl@iwhr.com (T.Q.); wengbs@iwhr.com (B.W.); biwx@iwhr.com (W.B.)
- <sup>4</sup> Department of Sociology and Social Work, School of Art & Sciences, National University of Mongolia, Ulaanbaatar 210646, Mongolia; otgonbayar\_ya@num.edu.mn
- <sup>5</sup> Department of Geography and Geology, School of Natural Science and Technology, Khovd State University, Khovd 164300, Mongolia; otgonbayar@khu.edu.mn
- <sup>6</sup> Department of Weather Forecast, National Agency for Meteorology Environment Monitoring, Ulaanbaatar 210646, Mongolia; tsasanchimeg@namem.gov.mn
- <sup>7</sup> Hydrology Division, The Information and Research Institute of Meteorology, Hydrology and Environment (IRIMHE), Ulaanbaatar 210646, Mongolia; oyunkhuu@irimhe.namem.gov.mn
- <sup>8</sup> College of Environmental Science and Engineering, Donghua University, Shanghai 201620, China; mohammedgedefaw@gmail.com (M.G.); abel.girma@uog.edu.et (A.G.); asaminewab@yahoo.com (A.A.)
- \* Correspondence: nyamdavaab@num.edu.mn (N.B.); yandh@iwhr.com (D.Y.); Tel.: +976-8010-2243 (N.B.); +86-10-6878-1976 (D.Y.)



**Citation:** Dorjsuren, B.; Batsaikhan, N.; Yan, D.; Yadambjav, O.; Chonokhuu, S.; Enkhbold, A.; Qin, T.; Weng, B.; Bi, W.; Demberel, O.; Boldsaikhan, T.; et al. Study on Relationship of Land Cover Changes and Ecohydrological Processes of the Tuul River Basin. *Sustainability* **2021**, *13*, 1153. <https://doi.org/10.3390/su13031153>

Received: 24 November 2020

Accepted: 24 December 2020

Published: 22 January 2021

**Publisher's Note:** MDPI stays neutral with regard to jurisdictional claims in published maps and institutional affiliations.



**Copyright:** © 2021 by the authors. Licensee MDPI, Basel, Switzerland. This article is an open access article distributed under the terms and conditions of the Creative Commons Attribution (CC BY) license (<https://creativecommons.org/licenses/by/4.0/>).

**Abstract:** The Tuul River Basin is the most important socioeconomic and political base area of Mongolia. Therefore, studying the interrelationships between changes in the ecohydrological processes of this basin and its land cover is of great importance for maintaining sustainability and the environment. This study investigated the annual average air temperature, total annual precipitation, and river discharge variability, and land cover changes at selected stations of the basin by using the hydrometeorological analysis, satellite analysis, and land cover determination statistical analysis. During the study period, the average annual air temperature rose from  $-1.5\text{ }^{\circ}\text{C}$  to  $+0.3\text{ }^{\circ}\text{C}$  ( $1.8\text{ }^{\circ}\text{C}$ ). The average annual precipitation exhibits relatively low change during this period. River discharge varied during the study period. A significant decreasing trend in river discharge was observed at the Terej ( $\varphi = -2.72$ ) and Ulaanbaatar ( $\varphi = -5.63$ ) stations, whereas the other stations, Altanbulag, Lun, and Orkhontuul, showed a significant increasing trend. During the study period, changes in land cover were directly related to main hydrometeorological parameters. Between 2000 and 2020, the amount of grassland decreased by  $319.67\text{ km}^2$ , while the area of water bodies increased by  $28.36\text{ km}^2$ . In the study area, mainly water bodies and sensitive areas of the land cover types were changed due to changes in precipitation. Studies in the arid and semiarid regions of Central Asia show that changes of ecohydrological processes have a significant impact on land cover changes.

**Keywords:** air temperature; precipitation; river discharge; climate change; land cover; water bodies; Mongolia

## 1. Introduction

The key indicator of global sustainability is measured by many factors, one of which is ecohydrological processes [1,2]. The cause and effect of ecohydrological changes depend on changes in its variables and it can affect several forms. It plays a major role in determining the hydrologic cycle, ecology, biogeochemical processes, soil moisture, river discharge changes, land cover changes, water quality, material flow (mainly due to the soil), vegetation, climate, and human activities [3]. Therefore, it is important to monitor, evaluate, and take steps to improve these processes in the areas of natural, social, and economic importance. It is important to study ecohydrological processes changes in the most sensitive areas, one of which is the Lake Baikal Basin [4,5].

The Lake Baikal Basin is a large area and the geographical location and natural components vary significantly [5,6]. Therefore, it is meaningful to study the characteristics of ecohydrological processes in the basin. The largest sub-basin of this basin is the Selenge River Basin, which has a significant impact on the hydrological processes of Lake Baikal [7]. The hydrological system of the Selenge River Basin is influenced by natural and social factors [8]. One of its main tributaries is the Tuul River.

The Tuul River Basin is located in central Mongolia, extending within the densely populated capital city Ulaanbaatar, the main gold mining region of Zaamar, the croplands, and major livestock areas [9]. Therefore, the Tuul River Basin is one of Mongolia's key socioeconomic, urban, mining, and agricultural regions [8,10,11]. The study of ecohydrological process changes in the Tuul River Basin is very important to determine the changes in hydrological processes, in the basin, and to understand and improve its direct and indirect effects, together with water resources in the Lake Baikal Basin and Mongolia. To do this, natural and social factors must be considered in detail.

While social factors can be improved through human activity management, identifying and improving the effects of natural factors is a complex process. In an ecohydrological process, this natural connectivity dictates responses to climate change, land cover change, river discharge, and vegetation events, and must be studied in detail to understand resilience and sensitivity [12].

Therefore, it may be useful to consider the relationship between hydrometeorology factors (air temperature, precipitation, river discharge) and changes in land cover from the natural factors that influence the ecohydrological process. On one hand, it can be an effective basis for identifying direct and indirect ecological impacts of ecohydrological processes on plants, animals, soil cover, and public health [13,14].

On the other hand, it is important to determine the sensitivity (increase and decrease) of water contingents for water bodies, wetland, and permanent snow and ice of the land cover in the river basin. In other words, it has many benefits, such as determining how some ecohydrological parameter changes affect surface aquifers and detecting direct and indirect effects [15,16].

Therefore, the purpose of this study is to examine the interrelationships of ecohydrological processes in the Tuul River Basin, such as hydrometeorological trends and land cover changes. This study identifies and describes in detail the following: (i) hydrometeorology changes, (ii) land cover changes, and (iii) interrelationships of ecohydrological processes of the basin.

## 2. Materials and Methods

### 2.1. Study Area

The Tuul River Basin is located in central Mongolia ( $46^{\circ}35'33''$ – $48^{\circ}57'13''$  N,  $102^{\circ}48'5''$ – $108^{\circ}8'40''$  E). The Tuul River has an important role in maintaining the surrounding environment, ecology, and socioeconomy in central Mongolia, and flows into the Orkhon River, passing through key economic and political regions such as Ulaanbaatar and the Zaamar region [17,18]. The Tuul River is 717 km long with a catchment area of 49,617.39 km<sup>2</sup>, and has elevations ranging from 776 m to 2784 m (Figure 1).

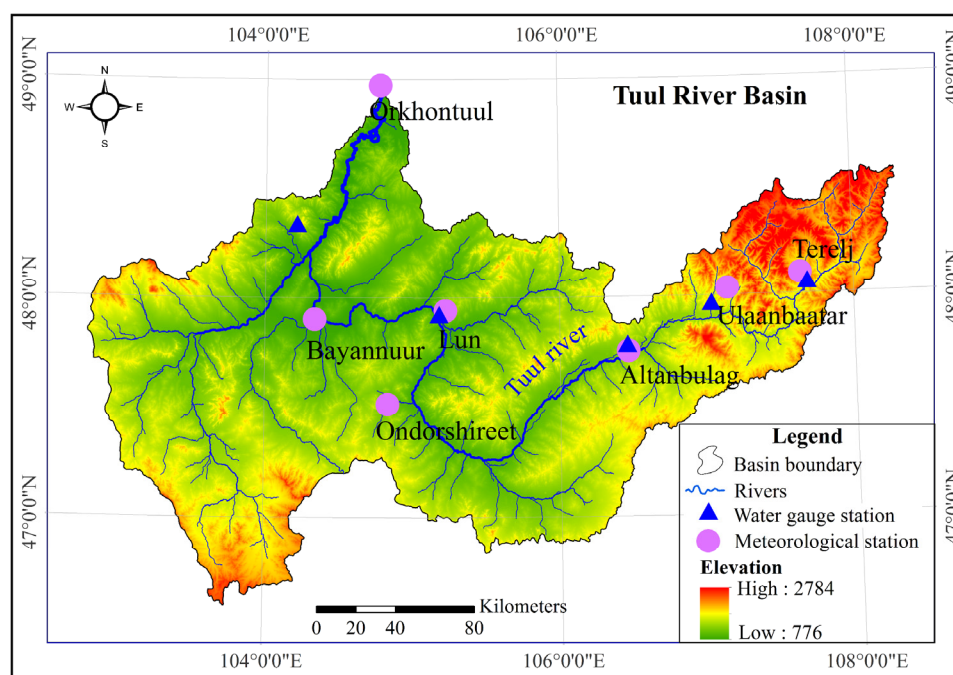


**Figure 1.** Location of the Tuul River Basin and stations.

## 2.2. Materials

Hydrometeorology data such as Tuul River Basin air temperature, precipitation, and river discharge were obtained from the Information and Research Institute of Meteorology, Hydrology and Environment. In addition, some data were obtained from NOAA's National Centers for Environmental Information (NCEI) (<https://ngdc.noaa.gov/>) to verify the data of some stations.

The soil map, topographic map, ecological landscape potential map, vegetation map, and forest map were selected for accuracy testing validation. Landsat Enhanced and Thematic Mapper (ETM+) and Landsat Thematic Mapper (TM) satellite data with a resolution of 30 m obtained for years 2000 to 2020 were employed for land cover classification. A global land cover dataset (GlobeLand30) product provides satellite data for land cover in the study area, which is from 2014 and described by the National Geomatics Center of China. All Landsat TM and ETM+ images derived from the USGS (<http://landsat.usgs.gov/>) were employed to interpret the spatial land cover situation during the previous 10 years.

## 2.3. Methods

Different trends in hydrometeorology variables (1979–2019) and land cover changes (2000, 2010, and 2020) were determined and relationships assessed using the innovative trend analysis method, Mann–Kendall test, Sen's slope estimator method, satellite imagery, and correlation calculations. To evaluate the reliability of the innovative trend analysis method (ITAM), the results were compared with the Mann–Kendall test (MK) and Sen's slope estimator test ( $\beta$ ). ArcGIS software was used to identify and process the land cover type (LC type). Transformation matrix (TM) of land covers were used to identify differences in land cover changes and to detect changes in water-related components. The relationship between hydrometeorology variables and land cover was determined by correlation and regression analysis based on various measurement data and statistical calculations (SC) (Figure 2).

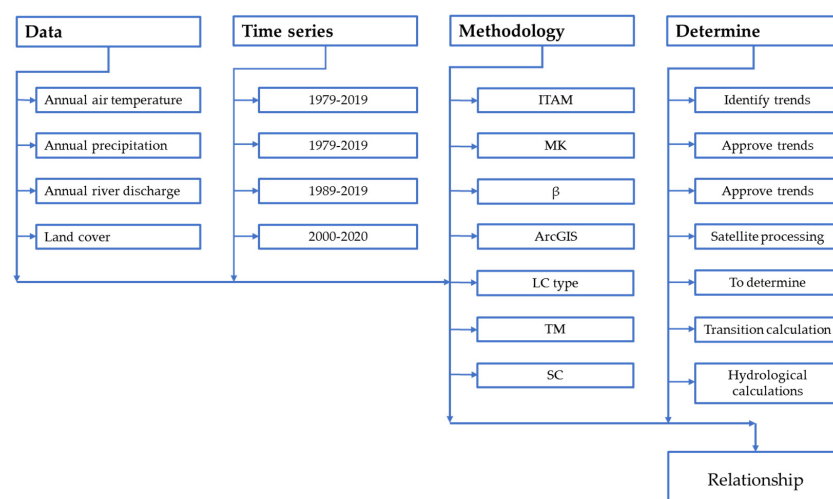


Figure 2. Scheme of methods.

### 2.3.1. Hydrometeorology Methods

The study of long-term trends in water and climate change allows us to identify and improve its causes and effects [19,20]. The following popular trend analysis methods, innovative trend analysis method, Mann-Kendall test, and Sen's slope estimator method, were used to detect the various trends of climate and river discharge in the periods from 1979 to 2019. In the study, significance levels at 10%, 5%, and 1% were taken to assess the hydrometeorology times series data. In this study, the trend of changes in annual average in air temperature, precipitation, and river discharge data were analyzed separately by the following methods.

The innovative trend analysis method divides a time series into two equal parts and it sorts both subseries in ascending order [21,22]. Following that, the two halves are placed on a coordinate system ( $x_i : i = 1, 2, 3, \dots, n/2$ ) on  $x$ -axis and ( $x_j : j = n/2 + 1, n/2 + 2, \dots, n$ ) on  $y$ -axis. If the time series data on a scattered plot are collected on a 1:1 ( $45^\circ$ ) straight line, it indicates no trend. On the other hand, the trend is increasing when data points accumulate above the 1:1 straight line and decreasing when data points accumulate below the 1:1 straight line. Mark the first half of the time series sorted along the ( $x_j$ ) axis and the second half of the time series along the ( $y_j$ ) axis (Figure 3).

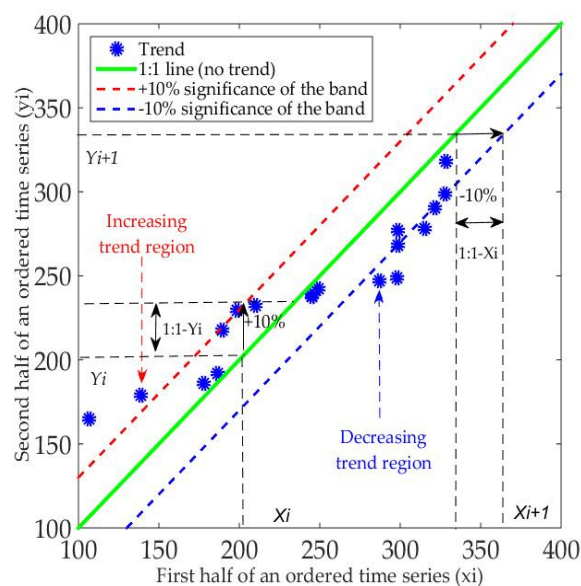


Figure 3. Image structure of the innovative trend analysis method.

The mean value difference among  $x_i$  and  $x_j$  give the trend magnitude of the data series. The ITAM indicator is expressed as:

$$\varphi = \frac{1}{n} \sum_{i=1}^n \frac{10(x_j - x_i)}{\mu} \quad (1)$$

where  $\varphi$  is the trend indicator,  $n$  is the number of each subseries, and  $\mu$  is the mean of the first data series. The value of  $\varphi$  is positive if it tends to increase. If the value is negative, it tends to decrease, and if  $i$  is between 1:1, it does not have a significant trend [23,24].

To evaluate the reliability of the innovative trend analysis method, the results were compared with the Mann–Kendall test and Sen's slope estimator test.

Mann–Kendall (MK) rank-based nonparametric statistical test applied in hydrometeorology studies is used for detecting trends in time series data [25]. It detects trends in a series without specifying whether the trend is linear or nonlinear. The variables  $S$  to be tested are calculated as:

$$S = \sum_{i=1}^{n-1} \sum_{j=i+1}^n \text{sgn}(x_j - x_i) \quad (2)$$

The trend test is applied to  $x_i$  data values ( $i = 1, 2, \dots, n-1$ ) and  $x_j$  ( $j = i+1, 2, \dots, n$ ). The value of each  $x_i$  is used as a reference point to compare with the value of  $x_j$ , which is given as:

$$\text{sgn}(x_j - x_i) = \begin{cases} +1 & \text{if } (x_j - x_i) > 0 \\ 0 & \text{if } (x_j - x_i) = 0 \\ -1 & \text{if } (x_j - x_i) < 0 \end{cases} \quad (3)$$

where  $x_j$  and  $x_i$  are the values in period  $j$  and  $i$ . When the number of data series is greater than or equal to ten ( $n \geq 10$ ), the MK test is then characterized by a normal distribution with the mean  $E(S) = 0$  and variance  $\text{Var}(S)$  equated as [26,27]:

$$E(S) = 0 \quad (4)$$

$$\text{Var}(S) = \frac{n(n-1)(2n+5) - \sum_{k=1}^m t_k(t_k-1)(2t_k+5)}{18} \quad (5)$$

where  $m$  is the number of the tied groups in the time series and  $t_k$  is the number of ties in the  $k$ th tied group.

The test statistic  $Z$  is:

$$Z = \begin{cases} \frac{s-1}{\delta} & \text{if } S > 0 \\ 0, & \text{if } S = 0 \\ \frac{s+1}{\delta} & \text{if } S < 0 \end{cases} \quad (6)$$

When  $Z$  is greater than zero, it indicates an increasing trend and when  $Z$  is less than zero, it is a decreasing trend [28].

The trend magnitude is calculated by Sen's slope estimator methods [21,23]. The slope  $Q_i$  between two data points is given by the equation:

$$Q_i = \frac{x_j - x_k}{j - k}, \text{ for } i = 1, 2, \dots, N \quad (7)$$

where  $x_j$  and  $x_k$  are data points at time  $j$  and ( $j > k$ ), respectively. When there is only a single datum in each time, then  $N = \frac{n(n-1)}{2}$ ;  $n$  is the number of time periods. However, if the number of data in each year is many, then  $N < \frac{n(n-1)}{2}$ ;  $n$  is the total number of observations. The  $N$  values of the slope estimator are arranged from smallest to largest. Then, the median of slope ( $\beta$ ) is computed as:

$$\beta = \begin{cases} Q[(N+1)/2] & \text{when } N \text{ is odd} \\ Q[(N/2) + Q(N+2)/(2)/(2)] & \text{when } N \text{ is even} \end{cases} \quad (8)$$



The sign of  $\beta$  shows whether the trend is increasing or decreasing.

### 2.3.2. Land Cover Methods

Spatial–temporal changes and impact analysis were performed by duplicating maps to determine changes in land cover over time and to establish correlations between land cover patterns. The magnitude of the land cover change is determined by comparing the satellite image at the beginning (2000) and end (2020) of the study period [5,29]:

$$CA = TA(t_2) - TA(t_1), \quad (9)$$

$$CE = [CA/TA(t_1)] * 100, \quad (10)$$

where  $TA$  is total area,  $CA$  is changed area,  $CE$  is the extent of change,  $t_1$  is beginning time, and  $t_2$  is ending time. Identified changes in land cover were calculated, along with the area size of the types of land cover transferred. To evaluate its accuracy, the modified area was confirmed using the kappa coefficient. In other words, the kappa coefficient is a statistical technique that was applied in the present study for assessing the accuracy of land cover changes. It confirms the agreement between predefined producer ratings and user-assigned ratings [30]:

$$K = P(A) - P(E)/1 - P(E), \quad (11)$$

$$P(A) = \frac{(A + D)}{N}, \quad (12)$$

$$P(E) = \left(\frac{A1}{N}\right) * \left(\frac{B1}{N}\right) + \left(\frac{A2}{N}\right) * \left(\frac{B2}{N}\right), \quad (13)$$

where  $K$  is the kappa coefficient,  $P(A)$  is the number of times the  $K$  raters agree,  $P(E)$  is the number of times the  $K$  rates are expected to agree only by chance,  $A$  and  $D$  are unchanged categories,  $A1$  and  $B1$  are subject's categories, and  $N$  is the change of results.

### 2.3.3. Analysis and Estimation of Hydrometeorology and Land Cover Variables Influence in the Tuul River Basin

Determining the relationship between hydrometeorological variables and land cover in the study area is important for understanding the ecohydrological process. To do this, it is important to establish the relationship between the various parameters of the water for statistical calculations and to identify the interrelationship between the interactions. From the hydrometeorological variables, the interaction between precipitation, air temperature, river discharge, and water bodies of land cover is calculated by the correlation and regression relationship [31,32].

## 3. Results and Discussion

### 3.1. Analysis of Hydrometeorology

The mean annual air temperature, mean annual precipitation, and average annual river discharge were calculated for each station on the study site by determining the long-term conditions of hydrometeorology change. Additionally, the correlations were calculated using the mean value of hydrological variables.

The result shows that the ITAM curve annual air temperature reveals a statistically sharp increasing trend in Ulaanbaatar from 1979 to 2019 ( $\varphi = 14.11$ ), a statistically abrupt increasing trend in Terelj from 1979 to 2019 ( $\varphi = 5.08$ ), a statistically upward trend in Altanbulag from 1979 to 2019 ( $\varphi = 2.82$ ), a statistically sharp upward trend in Ondorshireet from 1979 to 2019 ( $\varphi = 4.65$ ), a statistically sharp upward trend in Lun from 1979 to 2019 ( $\varphi = 3.29$ ), a statistically increasing trend in Bayannuur from 1979 to 2019 ( $\varphi = 4.25$ ); in Orkhontuul, a statistically increasing trend was observed with ( $\varphi = 4.75$ ) from 1979 to 2019. An overall statistically significant upward trend was observed in the average (five stations) ( $\varphi = 7.02$ ) (Figure 4). In the study period, the average annual air temperature rose from  $-1.5^\circ\text{C}$

to +0.3 °C (1.8 °C). This rise could have a direct and indirect significant effect on the ecohydrological processes of the arid and semiarid regions of Central Asia.

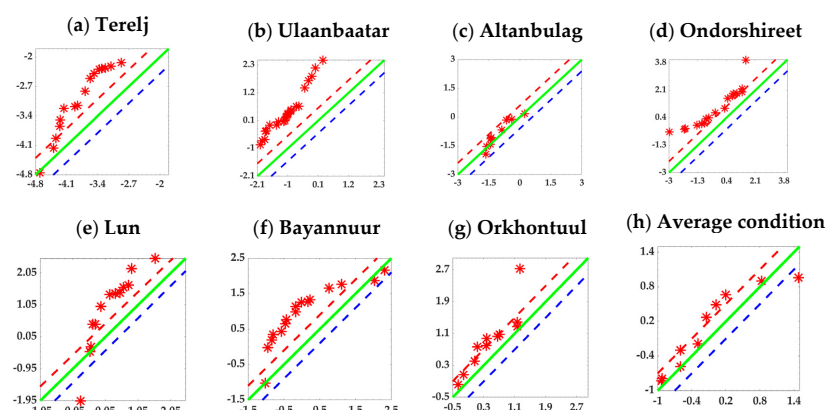


**Figure 4.** Trends of annual air temperature across stations, \* air temperature distribution

The trend analysis of annual air temperature for all stations is presented in Table 1.

**Table 1.** Results for air temperature trends: innovative trend analysis method ( $\varphi$ ), Mann–Kendall ( $Z$ ), and Sen’s slope estimator test ( $\beta$ ).

N <sup>o</sup>	Station	$\varphi$	$Z$	$\beta$
1	Terelj	5.08 ***	5.44 ***	0.06
2	Ulaanbaatar	14.11 ***	9.84 ***	0.06
3	Altanbulag	2.82 **	1.40 ***	0.04
4	Ondorshireet	4.65 ***	4.75 ***	0.08
5	Lun	3.29 ***	2.38 **	0.06
6	Bayannuur	4.25 ***	2.99 **	0.05
7	Orkhontuul	4.75 ***	0.92	0.01
8	Average	7.02 ***	1.46 *	0.04

\* Trends at 0.1 significance level. \*\* Trends at 0.05 significance level. \*\*\* Trends at 0.01 significance level.

The ITAM curve for mean annual precipitation reveals a statistically sharp downward trend in Terelj from 1979 to 2019 ( $\varphi = -2.44$ ); in Ulaanbaatar from 1979 to 2019 a downward trend ( $\varphi = -0.49$ ); a statistically increasing trend observed in Altanbulag ( $\varphi = 1.7$ ) and Ondorshireet from 1979 to 2019 ( $\varphi = 1.17$ ); a decreasing trend in Lun ( $\varphi = -0.27$ ); and increasing trend was observed in Bayannuur from 1979 to 2019 ( $\varphi = 1.38$ ); in Orkhontuul, an upward trend was obtained ( $\varphi = 0.96$ ). Overall, a slightly increasing trend was observed at the average condition ( $\varphi = 0.60$ ) (Figure 5). In the study period, the mean annual precipitation was 238 mm and the change was not significant.

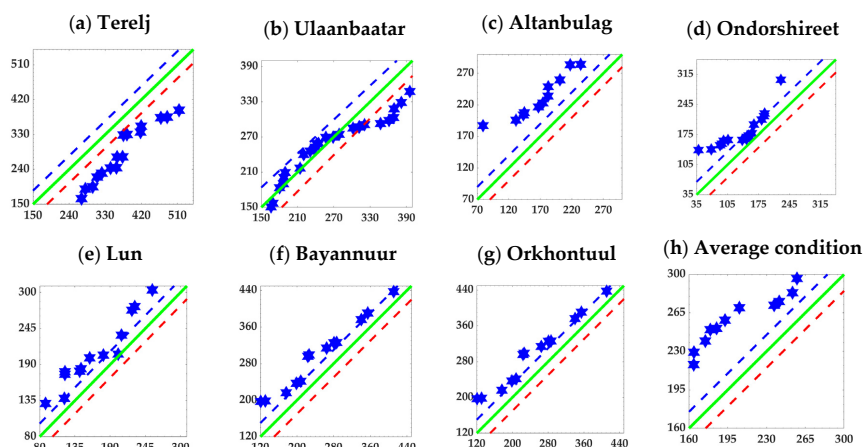


**Figure 5.** Trends of annual precipitation across stations, the stars are precipitation distribution.

The annual trend analysis of precipitation at all stations is presented in Table 2.

**Table 2.** Results of precipitation trends: innovative trend analysis method ( $\varphi$ ), Mann–Kendall (Z), and Sen’s slope estimator test ( $\beta$ ).

Nº	Station	$\varphi$	Z	$\beta$
1	Terelj	−2.44 **	−2.41 **	−3.29 ***
2	Ulaanbaatar	−0.49	1.25 *	0.55
3	Altanbulag	1.7 *	2.03 **	3.11 ***
4	Ondorshireet	1.17 *	4.99 ***	2.33 **
5	Lun	−0.27	1.80 *	3.03 ***
6	Bayannuur	1.38 *	2.02 **	1.84 *
7	Orkhontuul	0.96	0.61	1.57 *
8	Average	0.60	1.85 **	2.46 **

\* Trends at 0.1 significance level. \*\* Trends at 0.05 significance level. \*\*\* Trends at 0.01 significance level.

From 1989 to 2019, the ITAM curve mean annual river streamflow shows a statistically sharp downward trend in Terelj ( $\varphi = -2.72$ ), decreasing trend was observed in Ulaanbaatar ( $\varphi = -5.63$ ), and increasing trend was obtained at the Altanbulag, Orkhontuul, and Lun stations: ( $\varphi = 5.34$ ), ( $\varphi = 5.07$ ), and ( $\varphi = 3.42$ ), respectively. Overall, the average value for discharge shows a slightly increasing trend ( $\varphi = -0.92$ ) (Figure 6).

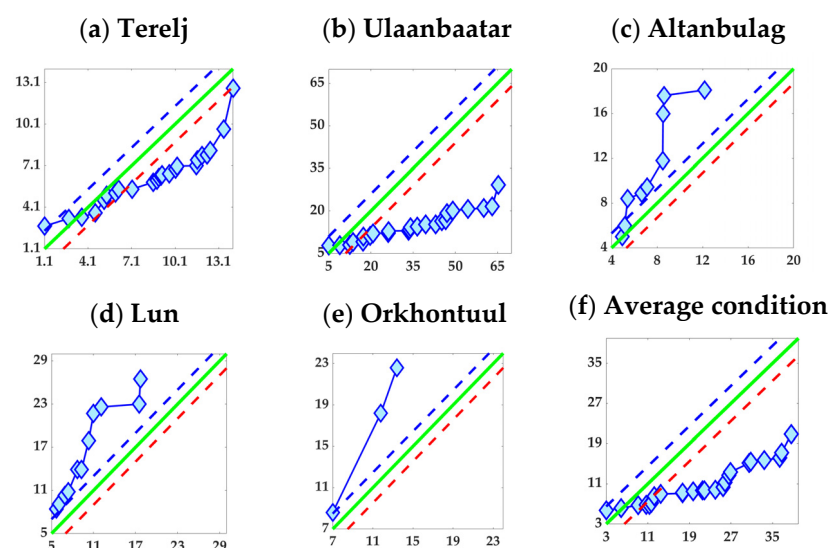


**Figure 6.** Trends of annual precipitation across stations, the rhombuses are river discharge distribution.

The annual trend analysis of river discharge for all stations is presented in Table 3.

**Table 3.** Results of river discharge trends: innovative trend analysis method ( $\varphi$ ), Mann–Kendall (Z), and Sen’s slope estimator test ( $\beta$ ).

Nº	Station	$\varphi$	Z	$\beta$
1	Terelj	−2.72 **	−3.03 ***	−35.56 ***
2	Ulaanbaatar	−5.63 ***	−3.32 ***	−144.12 ***
3	Altanbulag	5.07 ***	0.76	0.07
4	Lun	3.42 ***	1.29 *	119.47 ***
5	Orkhontuul	5.34 ***	0.43	2.13 **
6	Average	−0.92	−0.50	39.40 ***

\* Trends at 0.1 significance level. \*\* Trends at 0.05 significance level. \*\*\* Trends at 0.01 significance level.

### 3.2. Analysis of Land Cover

Determining land cover changes using satellite data is important because it allows us to determine land cover changes, shifts, and causes. Study areas were classified using two



commonly used supervised classification methods. The maximum-likelihood classification of the Tuul River Basin was used to analyze land cover maps for three different years (2000, 2010, and 2020). To confirm this, the results were compared with the soil, topographic, ecological landscape potential, vegetation, and forest maps. With appreciable accuracy, the Tuul River Basin landscape was classified according to eight land classes (Figure 7).

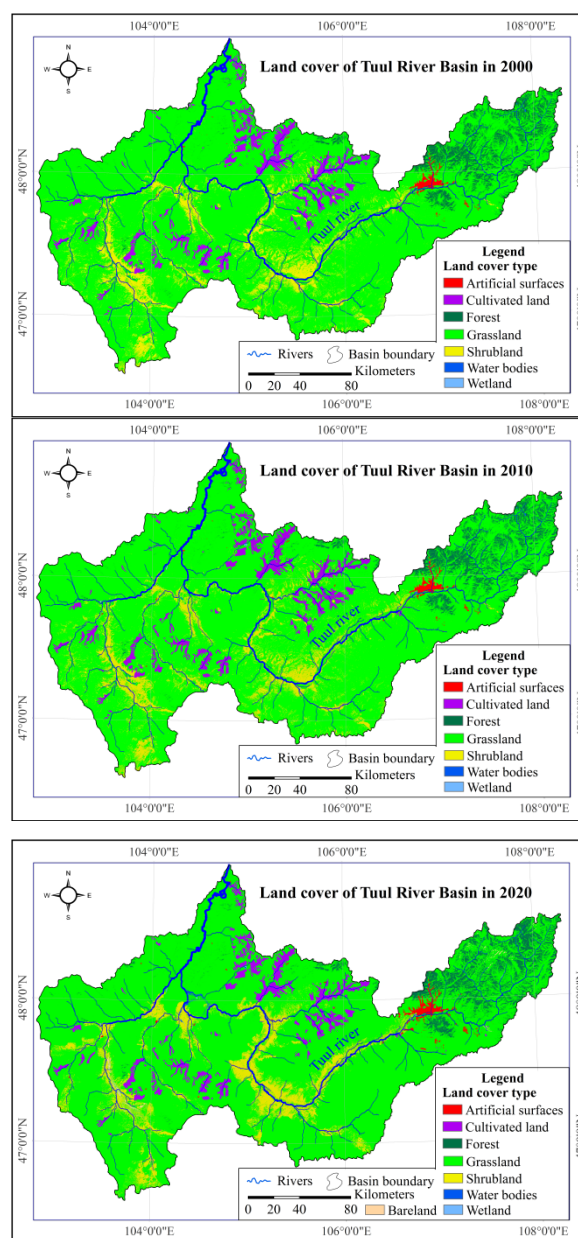


**Figure 7.** Land cover classification maps of the Tuul River Basin.

The number of classified pixels varied greatly in several types of land cover. It is noteworthy that most of the maximum changes occurred in the grassland and wetland area from 2000 to 2010. During those 10 years, the grassland area and wetland increased by 59.00 km<sup>2</sup> and 11.89 km<sup>2</sup>. In contrast, the water bodies and cultivated lands decreased by 45.89 km<sup>2</sup> and 28.00 km<sup>2</sup>. However, the change in land cover was even greater between 2010 and 2020, which was almost the opposite of the previous decade. The amount of grassland significantly decreased by −378.67 km<sup>2</sup> during the second decade, while the area of water bodies increased by 74.25 km<sup>2</sup> (Table 4).

**Table 4.** Land cover type and changed area.

Land Cover Types	Land Cover (2000)		Land Cover (2010)		Land Cover (2020)	
	Km <sup>2</sup>	%	Km <sup>2</sup>	%	Km <sup>2</sup>	%
Artificial surfaces (As)	204.50	0.41	208.30	0.42	307.03	0.62
Cultivated land (Cu)	2232.00	4.50	2204.00	4.44	2013.12	4.06
Forest (Fo)	1934.00	3.90	1937.00	3.90	2036.00	4.10
Grassland (Gr)	40,932.00	82.49	40991.00	82.61	40,612.33	81.85
Shrubland (Sh)	4222.00	8.51	4218.00	8.50	4410.14	8.89
Water bodies (Wb)	81.95	0.17	36.06	0.07	110.31	0.22
Wetland (We)	11.17	0.02	23.03	0.05	23.38	0.05
Bareland (Ba)					104.79	0.21
All types	49,617.62	100.00	49617.39	100.00	49,617.09	100.00

There was also a sharp increase in the size of the bareland, which was not evident in the previous decade. In this case, the high variability of the land cover indicates that there are some factors that strongly influence it.

During 2000 to 2010, the forms of land cover that are most sensitive to water changed significantly. Therefore, the study of land cover transitions and changes may be important in detecting the effects of change (Table 5).

**Table 5.** Transformation matrix of land cover from 2000 to 2010 (km<sup>2</sup>).

Land cover initial state (2000)									
Land cover initial state (2010)		Cu	Fo	Gr	We	Wb	As	Sh	Total
	Cu	2162.09	0.001	41.02		0.001	0.01	0.93	2204.05
	Fo	0.001	1916.88	5.21	0.04	2.04			1924.17
	Gr	69.95	1.67	40965.87	8.21	44.89	0.37	3.56	41094.52
	We		3.7	12	2.46	3.75	0.07	1.25	23.23
	Wb		0.48	4.14	0.43	29.16	0.01	0.93	35.15
	As	0.01	0.001	2.78		0.07	204.22	1.79	208.86
	Sh	0.22	0.001	1.73	0.32	1.03	0.04	4126.11	4129.45
Total		2232.27	1922.73	41032.76	11.45	80.94	204.71	4134.57	49619.43
Size			0–10		11–100		101–up		Total

Note: Background colors are the different sizes in the land cover area.

From 2000 to 2010, about 69.95 km<sup>2</sup> area of cultivated land was converted into grassland and 0.22 km<sup>2</sup> area of cultivated land was converted into shrubland. The conversion of forest land to grassland, wetland, and water bodies was 1.67 km<sup>2</sup>, 3.70 km<sup>2</sup>, and 0.48 km<sup>2</sup>, respectively. The conversion of grassland to cultivated land, forest, wetland, water bodies, artificial surfaces, and shrubland was 41.02 km<sup>2</sup>, 5.21 km<sup>2</sup>, 12.00 km<sup>2</sup>, 4.14 km<sup>2</sup>, 2.78 km<sup>2</sup>, and 1.73 km<sup>2</sup>, respectively. The conversion of wetland to grassland, water bodies, and shrubland was 8.21 km<sup>2</sup>, 0.43 km<sup>2</sup>, and 0.32 km<sup>2</sup>, respectively. The conversion of water bodies to forest land, grassland, wetland, and shrubland was 2.04 km<sup>2</sup>, 44.89 km<sup>2</sup>, 3.75 km<sup>2</sup>, and 1.03 km<sup>2</sup> respectively. The conversion of artificial surfaces to grassland, wetland, and shrubland was 0.37 km<sup>2</sup>, 0.07 km<sup>2</sup>, and 0.04 km<sup>2</sup>, respectively. The conversion of shrubland to cultivated land, grassland, wetland, water bodies, and artificial surfaces was 0.93 km<sup>2</sup>, 3.56 km<sup>2</sup>, 1.25 km<sup>2</sup>, 0.93 km<sup>2</sup>, and 1.79 km<sup>2</sup>, respectively. The most sensitive types of land cover are grassland and water bodies. The highest increase in land cover type was 59 km<sup>2</sup> for grassland and the highest decrease was 45.89 km<sup>2</sup> for water bodies. From 2000 to 2020, the forms of land cover that are most sensitive to temperature and water changed significantly (Table 6).

**Table 6.** Transformation matrix of land covers from 2000 to 2020 (km<sup>2</sup>).

		Land cover initial state (2000)							Total
Land cover initial state (2020)	As	199.10	2.77	0.07	96.63	8.70	0.07		307.33
	Ba		0.003	2.19	31.93	70.48	0.18	0.002	104.79
	Cu	0.01	1932.90	0.004	79.02	1.19	0.0002		2013.12
	Fo	0.08	0.003	1473.77	557.77	0.22	4.08	0.08	2036.00
	Gr	5.13	292.95	438.02	37658.46	2177.62	36.55	3.59	40612.33
	Sh	0.29	3.57	0.57	2531.30	1861.03	9.29	4.09	4410.14
	Wb	0.09	0.06	4.02	62.13	13.91	28.55	1.55	110.31
	We	0.01		3.71	14.03	1.11	2.26	2.24	23.38
Total		204.71	2232.25	1922.36	41031.27	4134.26	80.99	11.55	49617.39
Size			0–10		11–100		101–up		Total

Note: Background colors are the different sizes in the land cover area.

From 2000 to 2020, about 5.13 km<sup>2</sup> area of artificial surfaces land was converted into grassland. The conversion of cultivated land to artificial surfaces land, grassland, and shrubland was 2.77 km<sup>2</sup>, 292.95 km<sup>2</sup>, and 3.57 km<sup>2</sup>, respectively. The conversion of forest land to bareland, grassland, water bodies, and wetland was 2.19 km<sup>2</sup>, 438.02 km<sup>2</sup>, 4.02 km<sup>2</sup>, and 3.71 km<sup>2</sup>, respectively. The conversion of grassland to artificial surfaces land, bareland, cultivated land, forest land, shrubland, water bodies, and wetland was 96.63 km<sup>2</sup>, 31.93 km<sup>2</sup>, 79.02 km<sup>2</sup>, 557.73 km<sup>2</sup>, 2531.30 km<sup>2</sup>, 62.13 km<sup>2</sup>, and 14.03 km<sup>2</sup>, respectively. The conversion of shrubland to artificial surfaces land, bareland, cultivated land, grassland, water bodies, and wetland was 8.70 km<sup>2</sup>, 70.48 km<sup>2</sup>, 1.19 km<sup>2</sup>, 2177.62 km<sup>2</sup>, 13.91 km<sup>2</sup>, and 1.11 km<sup>2</sup>, respectively. The conversion of water bodies to forest land, grassland, shrubland, and wetland was 4.08 km<sup>2</sup>, 36.55 km<sup>2</sup>, 9.29 km<sup>2</sup>, and 2.26 km<sup>2</sup> respectively. The conversion of wetland to grassland, shrubland, and water bodies was 3.59 km<sup>2</sup>, 4.09 km<sup>2</sup>, and 1.55 km<sup>2</sup>, respectively. Numerous studies to estimate land cover displacement confirm the confidence value by the kappa coefficient [5,33–35]. If the accuracy value of the kappa coefficient classification is 0.61–0.80, it substantially ensures the accuracy of the land cover transition [36–38]. In this study, land cover classification for the years 2000 and 2020 was produced and the accuracy checked for the transformation matrix; the kappa coefficient was substantial, 0.78. This means that the estimates of land cover changes in the Tuul River Basin are accurate and interrelationships can be further analyzed.

### 3.3. Analysis of Interrelationships of Ecohydrological Processes

In the Tuul River Basin, air temperature statistically increased sharply at all stations, with Terelj ( $\varphi = 5.08$ ) and Ulaanbaatar ( $\varphi = 14.11$ ) the highest (Table 1). This greatly increases evaporation and has a direct effect on the reduction of water and moisture in the surface area. In the semiarid and arid regions of the Central Asian Plateau, precipitation is the main source of surface water, and surface water levels may increase as precipitation increases. It is important to examine whether there is a statistical relationship between hydrological processes and land cover components in the basin. This is especially important in understanding the ecohydrological process by establishing the relationship between river discharge and precipitation, and the components associated with the surface area of water bodies. In the study area, it was observed with a sharp increase in the average annual air temperature and a moderately negative correlation with a decrease in the water body type of land cover ( $r = -0.54$ ). It was observed that the average annual precipitation has a strong positive, statistically significant correlation with river water discharge ( $r = 0.70$ ). The interrelationships between the other sections were weak (Figure 8).

The ecohydrological processes in Mongolia are directly related to the amount of precipitation [39]. As a result of direct and indirect human and natural factors, the hydrological processes of Mongolia's major rivers are changing and river discharge is declining [40]. In particular, global warming increases evaporation and affects the land surface, decreasing the water surface [41]. Therefore, this may have had a significant impact on reducing

the surface area of water bodies ( $45.89 \text{ km}^2$ ) in the Tuul River Basin from 2000 to 2010. However, between 2010 and 2020, a slight increase in precipitation in the basin increased the area with water bodies ( $74.25 \text{ km}^2$ ). Between 2000 and 2020, the amount of grassland decreased by  $319.67 \text{ km}^2$ , while the area of water bodies increased by  $28.36 \text{ km}^2$ . In addition, due to temperature and evaporation, the amount of grassland area decreased and the amount of bareland increased. Therefore, it is important to establish an interrelationship by comparing the main hydrometeorological parameters, which have a major impact on the ecohydrological processes, with water bodies and sensitive areas of the land cover types (Figure 9).

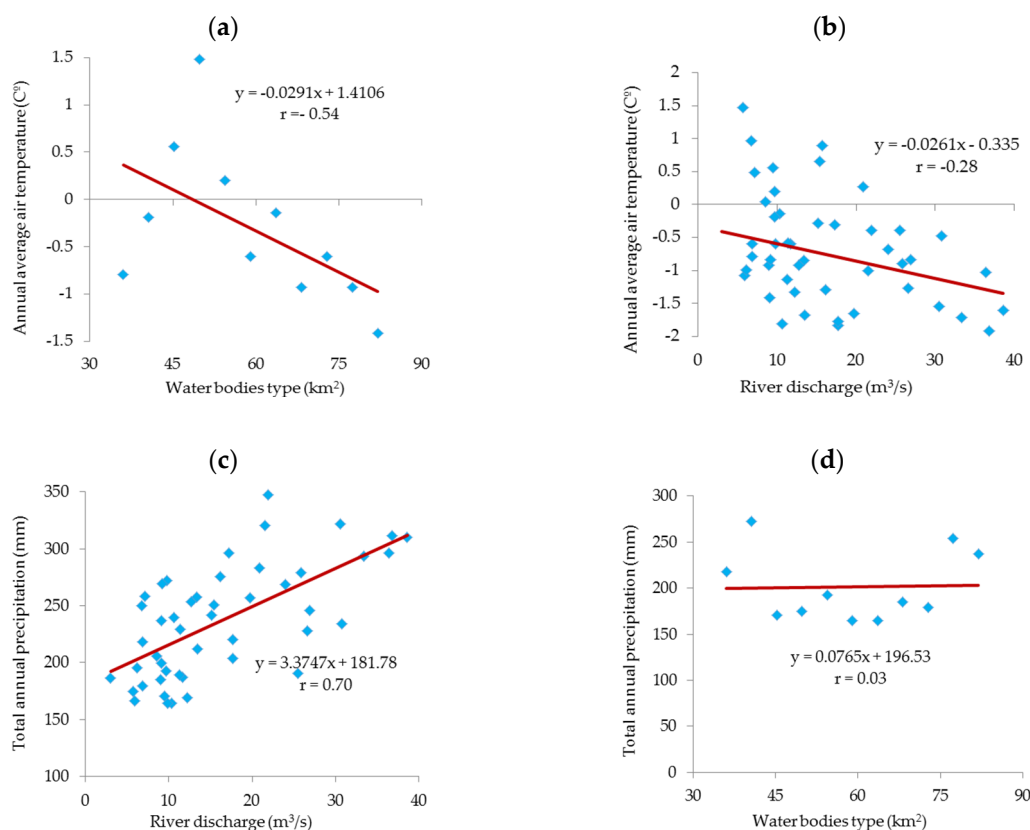


**Figure 8.** Regression between hydrometeorology and water variable interrelationships, such as (a) air temperature and water bodies type, (b) temperature and river discharge, (c) precipitation and river discharge, and (d) precipitation and water bodies type.

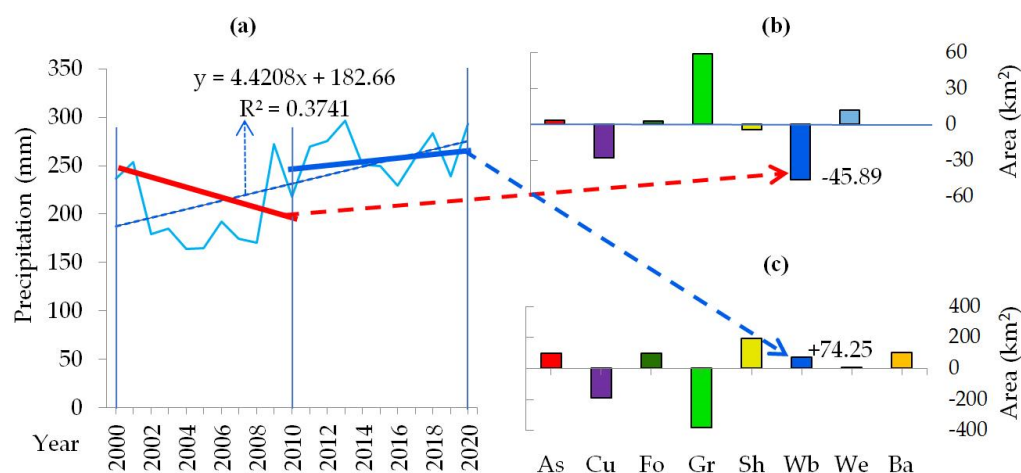


**Figure 9.** Interrelationships between precipitation and land cover in the Tuul River Basin between 2000 and 2020: (a) changes in precipitation, (b) changes in land cover between 2000 and 2010, and (c) changes in land cover from 2010 to 2020.

Studies in the arid and semiarid regions of Central Asia show that climate change has a significant impact on land cover changes [5,42]. When linking changes and shifts in this land cover to a hydrological system, it may be important to consider the spatial and temporal interrelationships of the key factors that affect it. In addition, changes in land cover have occurred in basin areas as a result of human and natural impacts (Figure 10).

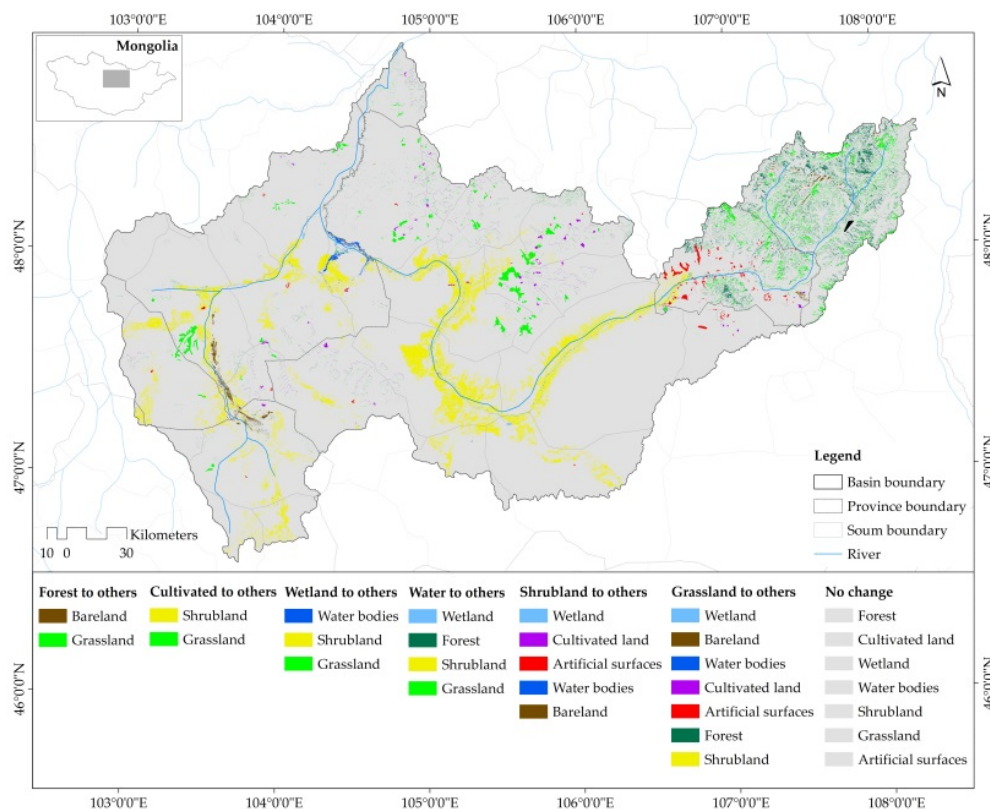


**Figure 10.** Land cover changes of the Tuul River Basin in 2000–2020.

The areas that changed the most were within the river zone. In particular, the size of grasslands along the river basin changed significantly and shifted to other forms. There is also a not less of a change in cultivated land and artificial surfaces that are changed by human activities. This is a manifestation of changes in the types of land cover due to human activities [43]. On the other hand, precipitation and water bodies of the basin are clearly declining due to global warming [44]. This is a natural factor affecting the land cover [45].

This baseline study is to determine the impact of climate change on ecohydrological processes, land cover changes, ecosystems, and surface aquifers in a semiarid region. It is consistent with the results of other studies on the hydrological processes and land cover of the Central Asian Plateau with a semiarid climate.

#### 4. Conclusions

In the Tuul River Basin, hydrometeorological variables, satellite data analysis and determination of land cover, and statistical analysis were used to calculate the values of the interrelationships of ecohydrological processes.

During the study period, the average annual air temperature rose from  $-1.5^{\circ}\text{C}$  to  $+0.3^{\circ}\text{C}$  ( $1.8^{\circ}\text{C}$   $361^{\circ}\text{C}$ ). This increase could have a significant effect on the ecohydrological processes and ecosystems of the arid and semiarid regions of Central Asia. The average annual air temperature showed a significantly increasing trend at all stations. In particular, Terelj ( $\varphi = 5.08$ ) and Ulaanbaatar ( $\varphi = 14.11$ ) had the highest increases. During the study period, the average annual precipitation was 238 mm. The average annual precipitation



change during this period was relatively small. A significant decreasing trend was observed at the Terelj ( $\varphi = -2.44$ ) and Ulaanbaatar ( $\varphi = -0.49$ ) stations, whereas the other stations, Altanbulag, Ondorshireet, Bayannuur, and Orkhontuul stations, demonstrated little increasing trend.

River discharge varied during the study period. A significant decreasing trend was observed at the Terelj ( $\varphi = -2.72$ ) and Ulaanbaatar ( $\varphi = -5.63$ ) stations, whereas the others stations, Altanbulag ( $\varphi = 5.07$ ), Lun ( $\varphi = 3.42$ ), and Orkhontuul ( $\varphi = 5.34$ ), demonstrated a significant increasing trend. The river discharge trend average condition decreased during the study periods ( $\varphi = -0.92$ ).

Changes in land cover varied in relation to hydrometeorological changes. It is noteworthy that most of the maximum changes occurred in the grassland and wetland area from 2000 to 2010. During those 10 years, the grassland area and wetland increased by 59.00 km<sup>2</sup> and 11.89 km<sup>2</sup>. In contrast, water bodies and cultivated lands decreased by 45.89 km<sup>2</sup> and 28.00 km<sup>2</sup>. However, the change in land cover was even greater between 2010 and 2020, which was almost the opposite of the previous decade. In other words, the amount of grassland decreased significantly by −378.67 km<sup>2</sup> during the study period, while the area of water bodies increased by 74.25 km<sup>2</sup>. Between 2000 and 2020, the amount of grassland decreased by 319.67 km<sup>2</sup>, while the area of water bodies increased by 28.36 km<sup>2</sup>. During the study period, changes in land cover were directly related to hydrometeorological main parameters. Water bodies and sensitive areas of the land cover types changed, mainly due to changes in precipitation in the study area. Studies in the arid and semiarid regions of Central Asia show that climate change has a significant impact on land cover changes.

This baseline study is to determine the impact of climate change on ecohydrological processes, land cover changes, ecosystems, and surface aquifers in a semiarid region.

**Author Contributions:** Conceptualization, B.D. and N.B.; methodology, O.Y.; software, B.D.; validation, S.C. and A.E.; formal analysis, W.B. and B.D.; investigation, B.W.; resources, T.Q.; data curation, O.G.; writing—original draft preparation, B.D.; writing—review and editing, W.B. and M.G.; visualization, A.A. and A.G.; supervision, O.D.; project administration, T.B.; funding acquisition, D.Y. All authors have read and agreed to the published version of the manuscript.

**Funding:** This work was supported by the Young Scientist Grant of the National University of Mongolia (grant: P2019-3732) with additional support from the National Key Research and Development Project of China (grant: 2016YFA0601503).

**Institutional Review Board Statement:** Not applicable.

**Informed Consent Statement:** Not applicable.

**Data Availability Statement:** Not applicable.

**Acknowledgments:** Special thanks to reviewers and editors who reviewed and provided valuable feedback on the quality of the final version of the article.

**Conflicts of Interest:** The authors declare no conflict of interest.

## References

1. Danielaini, T.T.; Maheshwari, B.; Hagare, D. Defining rural–urban interfaces for understanding ecohydrological processes in West Java, Indonesia: Part II. Its application to quantify rural–Urban interface ecohydrology. *Ecohydrol. Hydrobiol.* **2018**, *18*, 37–51. [\[CrossRef\]](#)
2. Taffarello, D.; Calijuri, M.d.C.; Viani, R.A.G.; Marengo, J.A.; Mendiondo, E.M. Hydrological services in the Atlantic Forest, Brazil: An ecosystem-based adaptation using ecohydrological monitoring. *Clim. Serv.* **2017**, *8*, 1–16. [\[CrossRef\]](#)
3. Krause, S.; Lewandowski, J.; Grimm, N.B.; Hannah, D.M.; Pinay, G.; McDonald, K.; Martí, E.; Argerich, A.; Pfister, L.; Klaus, J.; et al. Ecohydrological interfaces as hot spots of ecosystem processes. *Water Resour. Res.* **2017**, *53*, 6359–6376. [\[CrossRef\]](#)
4. Moreydo, V.; Millionshchikova, T.; Chalov, S. Modelling future hydroclimatic effects on the Coregonus migratorius spawning migration in the Selenga River and Lake Baikal. *Proc. Int. Assoc. Hydrol. Sci.* **2019**, *381*, 113–119.
5. Dorjsuren, B.; Yan, D.; Wang, H.; Chonokhuu, S.; Enkhbold, A.; Davaasuren, D.; Girma, A.; Abiyu, A.; Jing, L.; Gedefaw, M. Observed trends of climate and land cover changes in Lake Baikal basin. *Environ. Earth Sci.* **2018**, *77*, 725. [\[CrossRef\]](#)
6. Vladimirov, I.N. The ecological potential of Baikal region's geosystems. *IOP Conf. Ser. Earth Environ. Sci.* **2018**, *190*, 012017. [\[CrossRef\]](#)



7. Potemkina, T.; Sutyryna, E.; Potemkin, V. Changing of the riverine sediment load supply into Lake Baikal: The natural and anthropogenic causes (Russia). *Quat. Int.* **2019**, *524*, 57–66. [\[CrossRef\]](#)
8. Malsy, M.; Flörke, M.; Borchardt, D. What drives the water quality changes in the Selenga Basin: Climate change or socio-economic development? *Reg. Environ. Chang.* **2017**, *17*, 1977–1989. [\[CrossRef\]](#)
9. Fan, M. *Achieving Sustainable Integrated Water Resources Management in Mongolia: The Role of River Basin Organizations*; The Asian Development Bank: Manila, Philippines, 2020. [\[CrossRef\]](#)
10. Krueger, E.; Rao, P.S.C.; Borchardt, D. Quantifying urban water supply security under global change. *Glob. Environ. Chang.* **2019**, *56*, 66–74. [\[CrossRef\]](#)
11. Kasimov, N.; Karthe, D.; Chalov, S. Environmental change in the Selenga River—Lake Baikal Basin. *Reg. Environ. Chang.* **2017**, *17*, 1945–1949. [\[CrossRef\]](#)
12. Goodwell, A.E.; Kumar, P.; Fellows, A.W.; Flerchinger, G.N. Dynamic process connectivity explains ecohydrologic responses to rainfall pulses and drought. *Proc. Natl. Acad. Sci. USA* **2018**, *115*, E8604–E8613. [\[CrossRef\]](#) [\[PubMed\]](#)
13. Sun, G.; Hallema, D.; Asbjornsen, H. Ecohydrological processes and ecosystem services in the Anthropocene: A review. *Ecol. Process.* **2017**, *6*, 35. [\[CrossRef\]](#)
14. Andrade, E.M.; Guerreiro, M.J.S.; Palácio, H.A.Q.; Campos, D.A. Ecohydrology in a Brazilian tropical dry forest: Thinned vegetation impact on hydrological functions and ecosystem services. *J. Hydrol. Reg. Stud.* **2020**, *27*, 100649. [\[CrossRef\]](#)
15. Guo, Y.; Fang, G.; Xu, Y.-P.; Tian, X.; Xie, J. Identifying how future climate and land use/cover changes impact streamflow in Xinjiang Basin, East China. *Sci. Total Environ.* **2020**, *710*, 136275. [\[CrossRef\]](#)
16. Rodríguez-Morales, M.; Acevedo-Novoa, D.; Machado, D.; Ablan, M.; Dugarte, W.; Dávila, F. Ecohydrology of the Venezuelan páramo: Water balance of a high Andean watershed. *Plant Ecol. Divers.* **2019**, *12*, 573–591. [\[CrossRef\]](#)
17. Batbayar, G.; Pfeiffer, M.; von Tümpling, W.; Kappas, M.; Karthe, D. Chemical water quality gradients in the Mongolian sub-catchments of the Selenga River basin. *Environ. Monit. Assess.* **2017**, *189*, 420. [\[CrossRef\]](#)
18. Tsujimura, M.; Ikeda, K.; Tanaka, T.; Janchivdorj, L.; Erdenchimeg, B.; Unurjargal, D.; Jayakumar, R. Groundwater and surface water interactions in an alluvial plain, Tuul River Basin, Ulaanbaatar, Mongolia. *Sci. Cold Arid Reg.* **2013**, *5*, 0126–0132.
19. Pekel, J.-F.; Cottam, A.; Gorelick, N.; Belward, A.S. High-resolution mapping of global surface water and its long-term changes. *Nature* **2016**, *540*, 418–422. [\[CrossRef\]](#)
20. Piao, S.; Ciais, P.; Huang, Y.; Shen, Z.; Peng, S.; Li, J.; Zhou, L.; Liu, H.; Ma, Y.; Ding, Y.; et al. The impacts of climate change on water resources and agriculture in China. *Nature* **2010**, *467*, 43–51. [\[CrossRef\]](#)
21. Girma, A.; Yan, D.; Wang, H.; Song, X.; Qin, T.; Dorjsuren, B.; Gedefaw, M.; Abiyu, A.; Fikir, D.; Wang, J.; et al. Trends of Hydroclimate Variables in the Upper Huai River Basin: Implications of Managing Water Resource for Climate Change Mitigation. *Adv. Meteorol.* **2020**, *2020*, 8817068. [\[CrossRef\]](#)
22. Şen, Z. Hydrological trend analysis with innovative and over-whitening procedures. *Hydrol. Sci. J.* **2017**, *62*, 294–305. [\[CrossRef\]](#)
23. Wu, H.; Li, X.; Qian, H.; Chen, J. Improved partial trend method to detect rainfall trends in Hainan Island. *Theor. Appl. Climatol.* **2019**, *137*, 2539–2547. [\[CrossRef\]](#)
24. Nisansala, W.D.S.; Abeysingha, N.S.; Islam, A.; Bandara, A.M.K.R. Recent rainfall trend over Sri Lanka (1987–2017). *Int. J. Climatol.* **2020**, *40*, 3417–3435. [\[CrossRef\]](#)
25. Belihu, M.; Abate, B.; Tekleab, S.; Bewket, W. Hydro-meteorological trends in the Gidabo catchment of the Rift Valley Lakes Basin of Ethiopia. *Phys. Chem. Earth Parts A/B/C* **2018**, *104*, 84–101. [\[CrossRef\]](#)
26. Girma, A.; Qin, T.; Wang, H.; Yan, D.; Gedefaw, M.; Abiyu, A.; Batsuren, D. Study on Recent Trends of Climate Variability Using Innovative Trend Analysis: The Case of the upper Huai River Basin. *Pol. J. Environ. Stud.* **2020**, *29*, 2199–2210. [\[CrossRef\]](#)
27. Fathian, F.; Dehghan, Z.; Bazrkar, M.H.; Eslamian, S. Trends in hydrological and climatic variables affected by four variations of the Mann-Kendall approach in Urmia Lake basin, Iran. *Hydrol. Sci. J.* **2016**, *61*, 892–904. [\[CrossRef\]](#)
28. Wang, J. Determining the most accurate program for the Mann-Kendall method in detecting climate mutation. *Theor. Appl. Climatol.* **2020**, *142*, 847–854. [\[CrossRef\]](#)
29. Abate, T.; Angassa, A. Conversion of savanna rangelands to bush dominated landscape in Borana, Southern Ethiopia. *Ecol. Process.* **2016**, *5*, 6. [\[CrossRef\]](#)
30. Saha, S.; Paul, G.C.; Hembram, T.K. Classification of terrain based on geo-environmental parameters and their relationship with land use/land cover in Bansloi River basin, Eastern India: RS-GIS approach. *Appl. Geomat.* **2020**, *12*, 55–71. [\[CrossRef\]](#)
31. Boé, J.; Terray, L.; Habets, F.; Martin, E. Statistical and dynamical downscaling of the Seine basin climate for hydro-meteorological studies. *Int. J. Climatol.* **2007**, *27*, 1643–1655. [\[CrossRef\]](#)
32. Ebrahimi, A.; Nazemosadat, S.M.J.; Motamedvaziri, B.; Ahmadi, H. Land Use-Land Cover Change and Its Relationships with the Groundwater Table and the Plants' Altitudinal Zones: A Case Study of Arsanjan County, Iran. *Iran. J. Sci. Technol. Trans. Civ. Eng.* **2020**. [\[CrossRef\]](#)
33. Butt, A.; Shabbir, R.; Ahmad, S.S.; Aziz, N. Land use change mapping and analysis using Remote Sensing and GIS: A case study of Simly watershed, Islamabad, Pakistan. *Egypt. J. Remote Sens. Space Sci.* **2015**, *18*, 251–259. [\[CrossRef\]](#)
34. Zhang, X.; Liu, L.; Chen, X.; Gao, Y.; Xie, S.; Mi, J. GLC\_FCS30: Global land-cover product with fine classification system at 30 m using time-series Landsat imagery. *Earth Syst. Sci. Data Discuss.* **2020**, *2020*, 1–31. [\[CrossRef\]](#)
35. Dibs, H.; Hasab, H.A.; Al-Rifaie, J.K.; Al-Ansari, N. An Optimal Approach for Land-Use/Land-Cover Mapping by Integration and Fusion of Multispectral Landsat OLI Images: Case Study in Baghdad, Iraq. *Water Air Soil Pollut.* **2020**, *231*, 488. [\[CrossRef\]](#)

36. Gwet, K. Kappa statistic is not satisfactory for assessing the extent of agreement between raters. *Stat. Methods Inter-Rater Reliab. Assess.* **2002**, *1*, 1–6.
37. Viera, A.J.; Garrett, J.M. Understanding interobserver agreement: The kappa statistic. *Fam. Med.* **2005**, *37*, 360–363.
38. McHugh, M.L. Interrater reliability: The kappa statistic. *Biochem. Med.* **2012**, *22*, 276–282. [[CrossRef](#)]
39. Nakano, T.; Bat-Oyun, T.; Shinoda, M. Responses of palatable plants to climate and grazing in semi-arid grasslands of Mongolia. *Glob. Ecol. Conserv.* **2020**, *24*, e01231. [[CrossRef](#)]
40. Sukhbaatar, C.; Sodnom, T.; Hauer, C. Challenges for hydropeaking mitigation in an ice-covered river: A case study of the Eg hydropower plant, Mongolia. *River Res. Appl.* **2020**, *36*, 1416–1429. [[CrossRef](#)]
41. Konapala, G.; Mishra, A.K.; Wada, Y.; Mann, M.E. Climate change will affect global water availability through compounding changes in seasonal precipitation and evaporation. *Nat. Commun.* **2020**, *11*, 3044. [[CrossRef](#)]
42. Li, J.; Chen, H.; Zhang, C.; Pan, T. Variations in ecosystem service value in response to land use/land cover changes in Central Asia from 1995–2035. *PeerJ* **2019**, *7*, e7665. [[CrossRef](#)] [[PubMed](#)]
43. Chen, T.; Bao, A.; Jiapaer, G.; Guo, H.; Zheng, G.; Jiang, L.; Chang, C.; Tuerhanjiang, L. Disentangling the relative impacts of climate change and human activities on arid and semiarid grasslands in Central Asia during 1982–2015. *Sci. Total Environ.* **2019**, *653*, 1311–1325. [[CrossRef](#)] [[PubMed](#)]
44. Potemkina, T.G.; Potemkin, V.L.; Fedotov, A.P. Climatic factors as risks of recent ecological changes in the shallow zone of Lake Baikal. *Russ. Geol. Geophys.* **2018**, *59*, 556–565. [[CrossRef](#)]
45. Yin, J.; He, F.; Xiong, Y.J.; Qiu, G.Y. Effects of land use/land cover and climate changes on surface runoff in a semi-humid and semi-arid transition zone in northwest China. *Hydrol. Earth Syst. Sci.* **2017**, *21*, 183. [[CrossRef](#)]